# Investigation of the conditions of strong compact fracture

Andrey E. Buzyurkin[1a], Evgeny I. Kraus[1b], Yaroslav L. Lukyanov[2c]

[1]Khristianovich Institute of Theoretical and Applied Mechanics of Siberian Branch of RAS,

4/1 Instituskaya str., Novosibirsk, 630090, Russia,

[2]Lavrentyev Institute of Hydrodynamics of Siberian Branch of RAS,

15 Lavrentyev pr., Novosibirsk, 630090, Russia

[a]buzjura@itam.nsc.ru, [b]kraus@itam.nsc.ru, [c]lukyanov@hydro.nsc.ru

**Keywords:** shock waves, fracture, powder.

**Abstract.**
Methods of explosive loading of powder materials in conservation ampoules are applied in order to obtain new materials including composite ones with the unique physical and mechanical properties. In addition, these methods can be used to study phase transitions occurring in materials at high pressures and temperatures taking place behind shock waves, as well as for the synthesis of metastable phases.
In order to gain a better insight into the effect of loading conditions and, in particular, to study the effect of detonation velocity, explosive thickness, and explosion pressure on the properties of the final sample, we numerically solved the problem about powder compaction in the axisymmetric case.
The performed analysis shows that an increase in the decay time of the pressure applied to the sample due to an increase of the explosive thickness or the external loading causes no shrinkage of the destructed region at a fixed propagation velocity of the detonation wave. Simultaneously, a decrease in the propagation velocity of the detonation wave results in an appreciable shrinkage of this region.

## Introduction

Investigation into the interaction between oblique shock waves in porous materials and powders is a topical problem in optimization of loading conditions for obtaining, from a given sample, a compacted material with spatially uniform physical and mechanical properties. In compacting a powder in the cylindrical scheme, an irregular interaction between shock waves occurs. The compacted powder displays substantial non-uniformity in particle displacements, resulting in inhomogeneity of powder characteristics and, in some cases, even in material failure.
In compacting porous material and powders, the strong bonding between particles is achieved through the combined pressure-shear loading. During the compacting, a substantial energy is released at the interfaces between powder particles, resulting in surface cleaning and material melting in narrow interfacial regions. As a result, pore collapsing, giving rise to strong bonding between particles, occurs. Below, this phenomenon is termed compaction.
V.F. Nesterenko proposed the following criterion for the formation of a strong compact:

$$P > 2H_V, \tag{1}$$

where, according to [1], $H_V \approx 3Y_s$. Following [1], we can write criterion (1), deduced from experimental data, as

$$P > 6Y_s. \tag{2}$$

In turn, R. Prummer [2] uses the following condition for obtaining a uniform, in its physical properties, cylindrical compact with no Mach reflection induced singularities at its center: $P \approx H_V$, where $P$ is the detonation pressure. Comparing condition (1) with the condition $P \approx H_V$, Nesterenko [1] arrives at a conclusion that it is impossible in principle, without a central rod, to obtain a spatially uniform compact in the cylindrical loading scheme since the shock pressure required for obtaining a dense compact (2) will always lead to Mach reflection at the center of the sample.

Another important problem is preservation of the finish compact after loading. With the arrival of unloading waves, there arises a tensile stress that results in partial or complete destruction of the sample. We assume that the sample undergoes mechanical failure if the maximum tensile stress $\sigma_{max}$ reaches a certain critical value $\sigma_*$. In line with the adopted hypothesis, the following condition for the sample failure should be assumed:

$$\sigma_{max} > \sigma_*, \tag{3}$$

where $\sigma_{max}$ is the highest stress among the principal stresses for the strained state under study and $\sigma_*$ is the critical stress.

In the present work, the critical stress $\sigma_*$ is estimated as

$$\sigma_* = (2/3)Y_s ln(1/m_1),$$

where $m_1$ is the residual porosity. Taking the finish-compact density to equal $99\%$, we obtain $m_1 = 0.01$ and $\sigma_* \approx 3Y_s$. For the principal stresses, we have:

$$\sigma_1 = \frac{\sigma_{xx} + \sigma_{yy}}{2} + \frac{1}{2}\sqrt{(\sigma_{xx} - \sigma_{yy})^2 + 4\sigma_{xy}^2},$$

$$\sigma_2 = \frac{\sigma_{xx} + \sigma_{yy}}{2} - \frac{1}{2}\sqrt{(\sigma_{xx} - \sigma_{yy})^2 + 4\sigma_{xy}^2},$$

$$\sigma_3 = \sigma_{\theta\theta}.$$

**Calculation results and discussion**

In order to gain a better insight into the effect of loading conditions and, in particular, to study the effect of detonation velocity, explosive thickness, and explosion pressure on the properties of the final sample, we numerically solved the problem about powder compaction in the axisymmetric case. The problem statement is clear from Figure 1. We solved the full system of equations governing the deformation of a porous elastic-plastic material [3]. The action of the explosion products on the sample was modeled with a pressure applied to the upper border of the sample. The pressure was calculated by the approximation formula for the pressure upon unrestricted dispersion of detonation products [4]:

$$P(t) = P_H \exp(-(t - x/D)/t_1), \quad t_1 = \sqrt{\frac{3(\gamma_e + 1)}{4(\gamma_e - 1)}}\frac{\delta_e}{D}.$$

Here $\delta_e$ is the explosive thickness and $\gamma_e$ is the adiabatic exponent of the detonation products. At the lower border of the sample, the rigid-wall condition was set, and the right border was stress-free. At the left border, the rigid-wall condition was assumed.

In the calculations, the scheme proposed by Wilkins [5] for aluminum powders of various initial porosities was used.

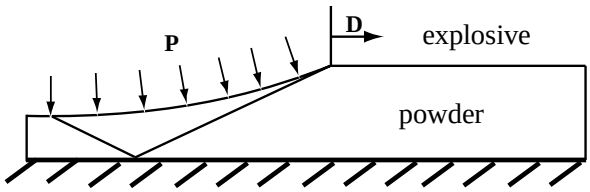


Fig.1. Problem statement.

Figure 2, a and b shows the pressure isolines for the cases of planar and cylindrical symmetries with identical loading conditions. It is seen from Fig. 2 that, in the planar statement of the problem, a regular reflection of the incident shock wave takes place. In the case of the cylindrical loading scheme, the incident shock waves bends as it approaches the cylinder axis, and, under the same loading conditions, an irregular reflection occurs.

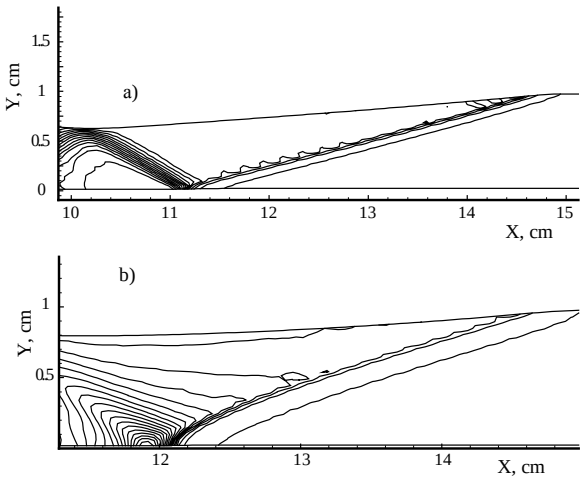


Fig.2. Pressure isolines: a) --- planar geometry; b) --- cylindrical configuration.

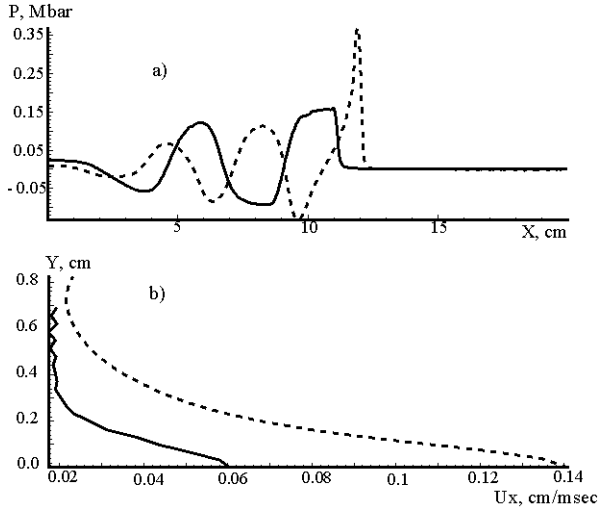


Fig.3. Pressure profile (a) and longitudinal-velocity profile $u_x(y)$ (b) for the planar and cylindrical geometries (solid and dashed lines, respectively).

Figure 3, a shows the pressure profile near the symmetry axis for the cases of planar and cylindrical statements (solid and dashed curves, respectively). An appreciable pressure rise near the symmetry axis is observed in the case of cylindrical configuration compared to the planar problem due to the divergence of the shock wave to the axis.

Figure 3, b shows the profile of the longitudinal velocity $u_x$ across the sample under loading behind the shock front. The solid and dashed lines show the data for the planar and axisymmetric problem statements, respectively. It is clearly seen that the velocity in the cylindrical case is much greater than in the planar variant.

As stated above, an important problem is preservation of finish compact, i.e., preventing its mechanical failure and obtaining a sample with uniform properties. Using criterion (3), we can find the interface between the solid and distructed materials. The regions of the compacted and porous materials for various explosive thicknesses for the external pressures $P = 0.05$ Mbar and $P = 0.075$ Mbar are shown in Fig. 4, a and b, respectively. In these calculations, the detonation velocity was $D = 0.5$ cm/$m$sec. The solid, dashed, and dot-and-dash lines outline the destruction regions for the explosive thicknesses $\delta_e = 2$ cm, $\delta_e = 3$ cm, and $\delta_e = 5$ cm, respectively. Region 1 is the

compacted region, and Region 2, the destruction region. An analysis of these graphs shows that an increase in the explosive thickness and, hence, an increase of the loading decay time does not cause any substantial shrinkage of the destruction region.

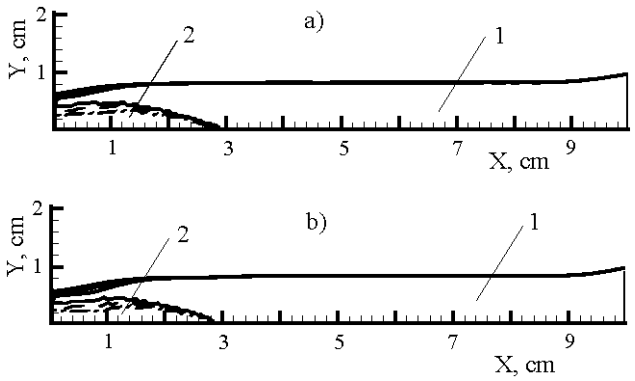


Fig.4. Compacted and destruction regions for various explosive thicknesses under external pressures $P = 0.05$ Mbar (a) and $P = 0.075$ Mbar (b). The detonation velocity is $D = 0.5$ cm/$m$ sec. The solid, dashed, and dot-and-dash lines refer to the explosive thicknesses $\delta_e = 2$ cm, $\delta_e = 3$ cm, and $\delta_e = 5$ cm, respectively. The compacted and destruction regions are indicated by 1 and 2.

It should be emphasized that this conclusion is valid for criterion (3). In derivation of (3), it was implicitly assumed that the interfacial melted zones are narrow, and the material in these zone rapidly solidifies as the particles in the bulk of the material undergo cooling. If this condition does not hold, then there can be a situation in which, by the moment of arrival of the unloading wave, the material in the interfacial zones still remains melted, which will prevent compaction. In this case, the dimensions of the destruction region will be dependent on the loading decay time and on the explosive thickness.

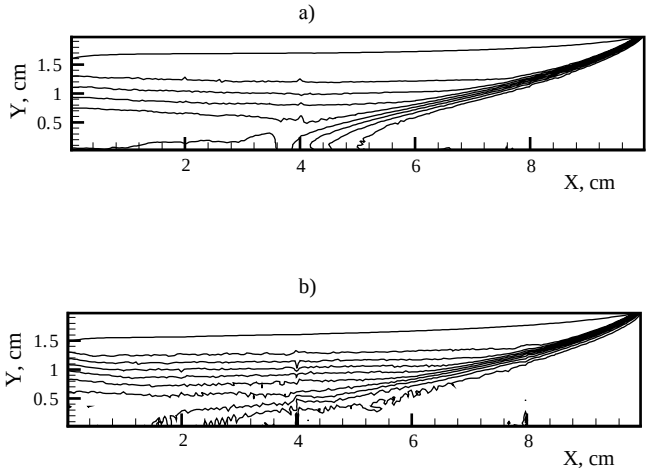


Fig.5. Density isolines for $\delta_e = 0.5$ cm: a) --- cylindrical configuration; б) --- planar statement.

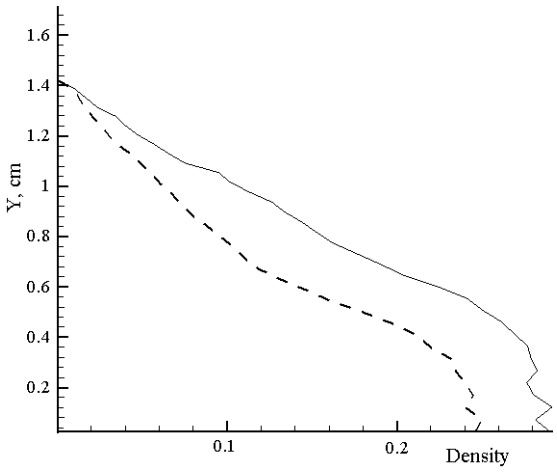


Fig.6. Porosity $m_1$ for $\delta_e = 0.5$ cm: solid line --- planar statement; dashed line --- cylindrical configuration.

The explosive thickness should be large enough to prevent shock wave damping in the powder and to enable complete pore collapsing in the sample. Figure 5, a and b shows the density isolines for the explosive thickness $\delta_e = 0.5$ cm and the external pressure $P = 0.05$ Mbar. Parts a and b of Fig. 5 depict the data for the axisymmetric and planar problem statements. Damping of the incident shock wave is evident from the figure. This results in incomplete powder compaction; the latter is clear from Fig. 6, which shows the distribution of porosity $m_1$ across the sample. The solid and dashed lines in this figure correspond to the planar case and to the cylindrical configuration, respectively. An analysis of these graphs shows that, in the axisymmetric case, due to the wave divergence to the axis, the pores undergo collapsing in a larger volume than in the planar variant.

A twofold increase in the explosive thickness makes the decay of the incidence shock wave less intensive. The density isolines for the explosive thickness $\delta_e = 1$ cm and the external pressure $P = 0.05$ Mbar are shown in Fig. 7, a and b. Parts a and b of this figure shows the calculation data for the axisymmetric and planar statements, respectively. It is clearly seen that in the case of cylindrical symmetry the shock wave bends near the axis, giving rise to an irregular reflection; in the planar configuration, a regular interaction occurs. Figure 8, which depicts the distribution of porosity $m_1$ across the sample compacted in the cylindrical geometry (the dashed line in Fig. 8), is indicative of complete collapsing of pores over the entire thickness of the sample. In the planar case (see the dashed line in Fig. 8), the complete collapsing of pores is observed approximately over half the thickness of the sample, and the porosity near the symmetry axis is close to the initial one, $m_1^0$.

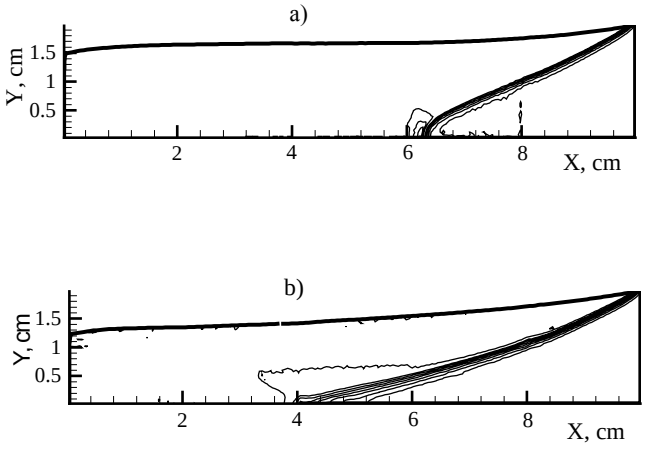


Fig.7. Density isolines for $\delta_e = 1$ cm: a) --- cylindrical configuration; b) --- planar configuration.

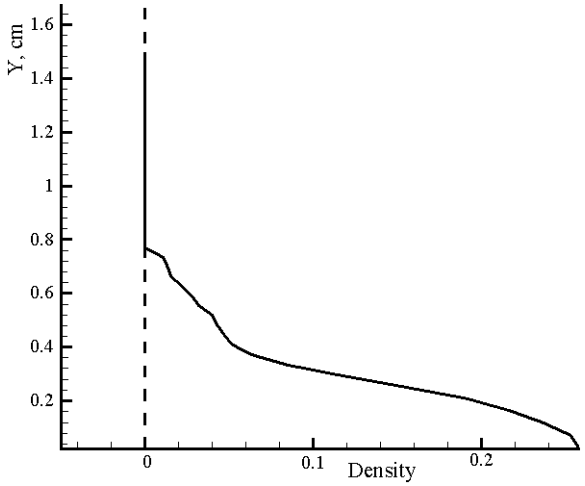


Fig.8. Porosity $m_1$ for $\delta_e = 1$ cm: solid line --- planar statement; dashed line --- cylindrical configuration.

The density isolines for the explosive thickness $\delta_e = 2$ cm are shown in Fig. 9, a and b. The external pressure was taken to be $P = 0.05$ Mbar. Parts a and b of this figure show the calculation data for the axisymmetric and planar statements. In the cylindrical case (see Fig. 9, a), an irregular reflection is clearly observed, whereas in the planar case (see Fig. 9, b) the incident shock wave interacts with the rigid wall in the regular manner. In both cases, all pores in the sample collapse completely.

Further calculations were carried out for the explosive thicknesses $\delta_e = 2$ cm, $\delta_e = 3$ cm, and $\delta_e = 5$ cm.

Figure 10, a and b illustrates the effect of applied pressure on the dimensions (thickness?) of the destruction region. In the calculations, the external pressures were $P = 0.05$ Mbar and $P = 0.075$

Mbar, respectively, and the detonation velocity in both cases was $D = 0.7$ cm/$m$ sec. The solid and dashed lines show the data for the explosive thicknesses $\delta_e = 3$ cm and $\delta_e = 5$ см. Regions 1 and 2 are the compacted and destruction regions. As is seen from the figure, an increase in the external load causes no shrinkage of the destruction zone. Thus, it can be concluded that an increase in the decay time of the pressure applied to the sample resulting from an increase in the explosive thickness or in the value of the external load does not make the destruction zone shrink at a fixed propagation velocity of the detonation wave.

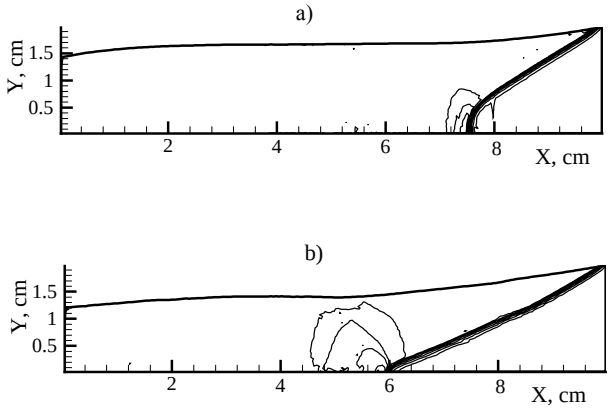


Fig.9. Density isolines for $\delta_e = 2$ cm: a) --- cylindrical configuration; b) --- planar statement.

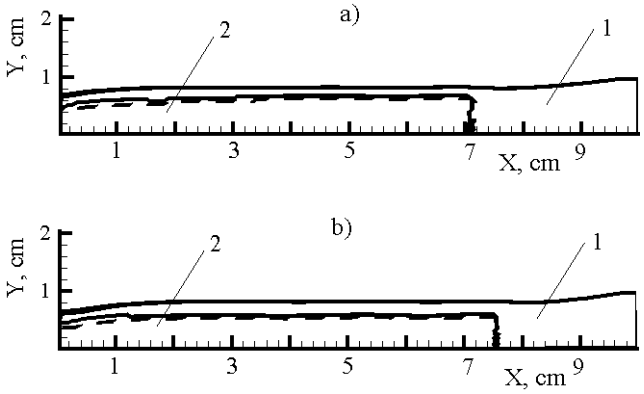


Fig.10. Compacted and destructed regions for two values of external pressure, $P = 0.05$ Mbar (a) and $P = 0.075$ Mbar (b). The detonation velocity is $D = 0.7$ cm/$m$ sec. The solid and dashed lines show the calculation data for the explosive thicknesses $\delta_e = 3$ cm and $\delta_e = 5$ см.

A decrease in the velocity of the detonation wave results in a considerable shrinkage of the destruction region. Figure 11 show the compacted (1) and destructed (2) regions in the sample for the detonation velocities $D = 0.3,\ 0.5,\ 0.7$ cm/$m$ sec at a fixed explosive thickness $\delta_e = 5$ cm and at a fixed external pressure $P = 0.05$ Mbar. The solid, dashed, and dot-and-dash lines show the calculation data for the detonation velocities $D = 0.3$ cm/$m$ sec, $D = 0.5$ cm/$m$ sec, and $D = 0.7$ cm/$m$ sec.

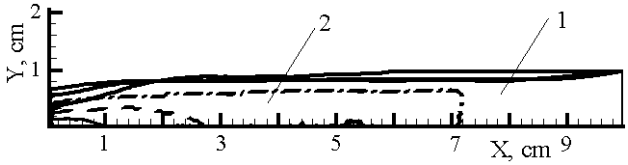


Fig.11. Compacted (1) and destructed (2) regions for three values of the detonation velocity. The solid, dashed, and dot-and-dash lines refer to $D = 0.3$ cm/$m$ sec, $D = 0.5$ cm/$m$ sec, and $D = 0.7$ cm/$msec$.

The isolines of pressure for the indicated loading parameters are shown in Figure 12, a--c. It is seen from the graphs that, as the shock-wave propagation velocity increases, the angle of incidence decreases and the reflected shock causes material destruction (see Fig. 12, b and c). As the velocity of the detonation wave increases, the angle of incidence of the incident shock wave increases and, as

it is seen from Fig. 12, a, at the velocity $D = 0.3$ cm/$m$ sec the incident shock wave is close to the normal shock and the amplitude of the reflection wave is almost zero.

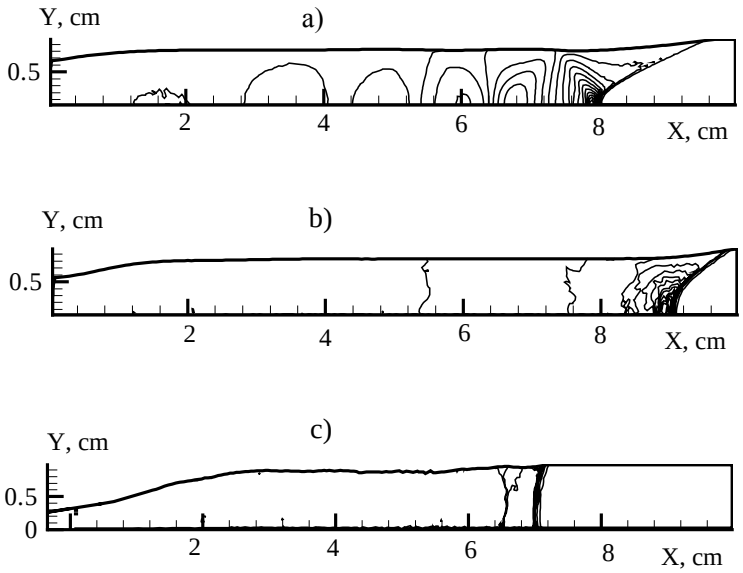


Fig.12. Pressure isolines: a) --- detonation velocity $D = 0.7$ cm/$m$ sec; b) --- detonation velocity $D = 0.5$ cm/$m$ sec; c) --- detonation velocity $D = 0.3$ cm/$m$ sec

Since in the case of cylindrical symmetry no regular reflection occurs, the final sample turns out to be inhomogeneous. Figure 13 shows the distribution of the longitudinal velocity $u_x$ (рис. 13, a) and temperature $T$ (рис. 13, b) across the sample in the compacted region for the detonation velocity $D = 0.5$ cm/$m$ sec. An appreciable non-uniformity in the distribution of parameters is evident from the graphs. Near the axis, both the velocity and temperature are greater than in the region some distance away from it.

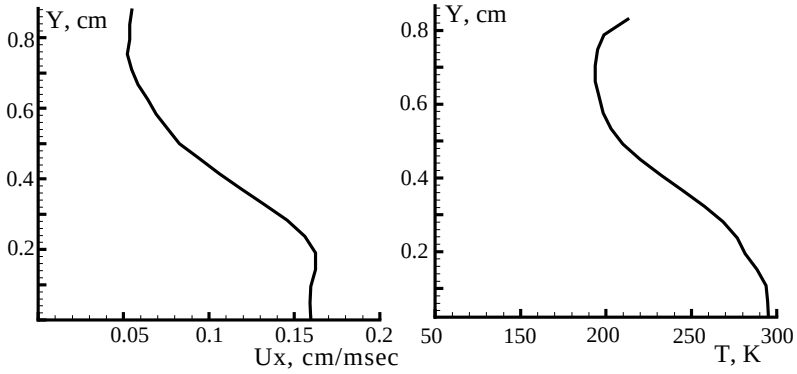


Fig.13. Predicted distributions of the longitudinal velocity $u_x$ (a) and temperature $T$ (b) across the compacted region of the sample for the detonation velocity $D = 0.5$ cm/$m$ sec.

Parts a and b of Fig. 14 show the distributions of the longitudinal velocity $u_x$ and temperature $T$ across the compacted region of the sample predicted for the detonation velocity $D = 0.3$ cm/$m$ sec. Here, under identical loading parameters, the final sample is quire homogeneous.

As a result, it becomes possible to obtain spatially uniform compacted samples. The necessary condition for this is sufficiently low detonation velocity, equal, for the aluminum powder, to $0.3$ cm/$m$sec. Here, on the one hand, compaction condition (1) should be fulfilled and, on the other, the uniformity of loading parameters across the sample should be ensured.
Thus, the compaction of powders with low detonation velocities results in a considerable shrinkage of destruction zones in finish samples and in spatial uniformity of material parameters in their compacted parts.

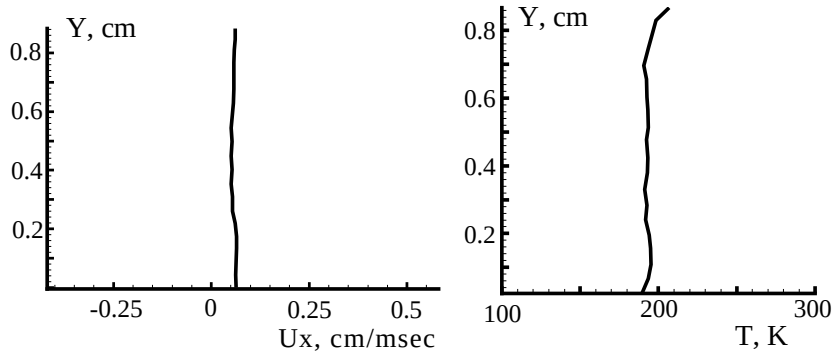


Fig.14. Distributions of the longitudinal velocity $u_x$ (a) and temperature $T$ (b) across the compacted region of the sample for the detonation velocity $D = 0.3$ cm/$m$ sec.

The performed analysis shows that an increase in the decay time of the pressure applied to the sample due to an increase of the explosive thickness or the external loading causes no shrinkage of the destructed region at a fixed propagation velocity of the detonation wave. Simultaneously, a decrease in the propagation velocity of the detonation wave results in an appreciable shrinkage of this region.

**Conclusions**

The following conclusions can be drawn from the present study of powder compaction under shock pressing in the axisymmetric case. An increase in the pressure decay time due to increasing either the explosive thickness or the external loading intensity causes no shrinkage of the destruction zone at a fixed propagation velocity of the detonation wave. Compaction of powders with low detonation velocities results in a considerable shrinkage of destruction zones in finish samples and in a uniform distribution of material parameters in the compacted region.

**Acknowledgment**

This work was supported by a grant of the President of the Russian Federation for State Support of Leading Scientific Schools of Russia 1541.2012.1

**References**

[1] V.F. Nesterenko: *High-rate deformation of heterogeneous materials* (Nauka, Novosibirsk 1992) (in Russian).
[2] R. Prümmer: *Powder compaction. Explosive welding, forming and compaction* (London; New York: Appl. Sci. Publ., 1983).
[3] S.P. Kiselev, V.M. Fomin: PMTF. no. 6 (1993), pp. 125-133 (in Russian).
[4] V.V. Pai, G.E. Kuz'min, I.V. Yakovlev: Combustion, Explosion, and Shock Waves, Volume 31, No.3. (1995), pp.124-130.
[5] M.L. Wilkins: *Computer simulation of dynamic phenomena (*Springer, Berlin, Heidelberg 1999)